Journal of Materials Chemistry A

ROYAL SOCIETY OF CHEMISTRY

PAPER

View Article Online
View Journal

Cite this: DOI: 10.1039/d6ta01538g

Electrolyte effects on the stability and CO binding of copper chloride complexes for electrochemical separation of CO/N_2

Christel I. Koopman,[ab] Jelco Albertsma,[a] Zhengyao Zhu,[ab] Monique A. van der Veen[a] and David A. Vermaas[*ab]

Carbon monoxide separation from industrial waste gases could contribute largely to carbon circularity. Traditional separation technologies are unable to separate CO from N_2 selectively. Instead, electroactive carriers show promise in selective separation of CO from N_2, where CO binds a complex in one oxidation state and releases in another oxidation state. We study Cu(I)/Cu(II)-chloride complexes as potential carrier materials with high binding affinity to CO, good solubility and low energy consumption of the process. We show that the electrolyte composition of a copper chloride system affects the binding affinity and stability of the copper carrier (Cu^+). Cyclic voltammetry measurements reveal that the CO binding constant increase from the previously reported 1600 M^{-1} for 1 M KCl to 5500 M^{-1} for 0.5 M $CaCl_2$. However, this increase in binding constant is not reflected to the same extent in the CO capture capacity, showing a smaller increase in CO capture. In general, the binding constant decreases with chloride concentration, while the Cu^+ stability window increases. This highlights a trade-off that needs to be considered for electrolyte selection in electrochemical CO separation with copper chlorides.

Received 20th February 2026
Accepted 8th April 2026

DOI: 10.1039/d6ta01538g

rsc.li/materials-a

Introduction

Separation of carbon monoxide (CO) could be an important part of carbon circularity within the chemical industry, as CO is both an essential feedstock and a common by-product in chemical processes, such as steel manufacturing.[1–3] However, the CO in waste gases (ranging in concentrations from 5 to 80 vol%)[4] is burned for energy generation and emitted as CO_2 into the environment. Instead, recycling of the CO in industrial waste gases could provide a valuable resource of CO while also reducing CO_2 emissions. It is estimated that recycling of CO from the steel industry would reduce the total anthropogenic CO_2 emissions by about 1–2%.[2,5] However, currently this potential feedstock is lost due to the absence of suitable separation methods to recycle CO from waste gases. Especially the separation from nitrogen (N_2) has remained a challenge due to similar physical properties in molecular mass, boiling point and size.[4]

Instead, affinity-based separation could provide options for CO/N_2 separation. CO is known to have a strong affinity to transition metals, such as the Fe^+ in hemoglobin (220 times greater than O_2).[6] CO can bind to transition metals through a combination of σ-donation of electrons from the CO ligand to the metal and π-backbonding from the metal to the π*-antibonding orbital of the CO. Especially, the π-backbonding contributes to the high affinity of CO to transition metals and generally increases for electron-rich metals.[7–11] As a result, the lower oxidation state is expected to have a stronger affinity to CO than the higher oxidation state, which can be leveraged in an electrochemical separation process.

Recent previous work showed a proof-of-concept for CO capture from mixed gases with Ni-based redox couples[12] and Terry *et al.* have demonstrated electrochemical separation of CO from N_2 with a copper chloride absorbent.[13] The latter process uses two electrochemical cells and two contacting units to capture and release CO. Here, copper is reduced to its high-affinity state (Cu^+) to then absorb CO from a feed reservoir and is subsequently oxidised back to the low-affinity state (Cu^{2+}) to release CO in a receiving reservoir. Their carrier solution (0.025 M copper chlorides, 1.0 M KCl and 0.1 M HCl) has a CO binding constant of 1600 M^{-1} and successfully separates and concentrates CO from N_2.

While this previous work shows the potential of copper chloride carriers for electrochemical CO separation, it also exhibits low energy efficiencies due to slow kinetics and low carrier utilisation. For this technology to become a potential separation method to recover CO from industrial waste gases, high CO recovery and product purity at a low energy consumption are required. The carrier material is determining for the performance of this separation process through its solubility, stability, and CO binding affinity. While we know that the carrier's binding constant is pivotal to make this technology

[a]Department of Chemical Engineering, Delft University of Technology, Van der Maasweg 9, Delft, 2629HZ, The Netherlands. E-mail: d.a.vermaas@tudelft.nl
[b]e-Refinery Institute, Leeghwaterstraat 39, Delft, 2628CB, The Netherlands

more competitive in selectivity and energy efficiency, we currently lack insight into how the binding constant is controlled for Cu^+/Cu^{2+} electro-swing absorption. Previous work demonstrated that transition metal complexes are capable of having high CO binding affinities up to 10^5 M^{-1}.[14,15] We aim to find opportunities to improve the binding constant of aqueous copper chloride solutions from the reported 1600 M^{-1}.[13] This requires understanding of the binding between CO and the electro-active carrier and the effect of its solution environment to optimise for high binding affinity.

Therefore, this work aims to understand the effect of the electrolyte composition on the binding affinity and carrier stability of an aqueous copper chloride carrier. We use DFT and Visual Minteq to predict CO affinity of copper chloride solutions and perform cyclic voltammetry measurements to estimate the binding constant and Cu^+ stability of the different carrier solutions. We demonstrate electrochemical separation of CO through capture and release in an H-cell for different mixed CO/N_2 gas feeds.

Background

The importance of K_{CO}

The binding constant is a measure of affinity and is described by the equilibrium between a carrier and a ligand. The material's affinity to the different gas components will determine the performance of the separation process, for example in terms of selectivity and capacity utilisation. A higher binding constant means more of the dissolved gas species is bound to the carrier material, following eqn (1) for CO and Cu^+.

$$K_{CO} = \frac{[Cu^+CO]}{[Cu^+][CO]} \quad (1)$$

Here K_{CO} represents the binding constant between the carrier Cu^+ and the ligand CO, assuming the binding of one CO. The binding constant can provide theoretical upper limits for selectivity and capacity utilisation at equilibrium, as described in eqn (2) and (3) for CO/N_2 separation (derived in SI-1).

$$\alpha = \frac{[CO]_{tot}/P_{CO}}{[N_2]_{tot}/P_{N_2}} = \frac{H_{CO}}{H_{N_2}}\left(1 + \frac{K_{CO}[Cu^+]_{tot}}{1 + K_{CO}H_{CO}P_{CO}}\right) \quad (2)$$

$$\text{Capacity utilisation} = \frac{[Cu^+CO]}{[Cu^+]_{tot}} = \frac{K_{CO}H_{CO}P_{CO}}{1 + K_{CO}H_{CO}P_{CO}} \quad (3)$$

Here, $[CO]_{tot}$ and $[N_2]_{tot}$ are the total concentration of dissolved CO and N_2, including dissolution of the gases in the solvent and CO bound to the carrier, $[Cu^+]_{tot}$ is the total carrier concentration, P_i is the partial pressure and H_i is the Henry constant of gas component i in the solvent. The first term on the right-hand side of eqn (2) reflects the solubility of gases in the solvent, while the latter term reflects the CO bound to the Cu^+ carrier.

Fig. 1 shows the theoretical selectivity and capacity utilisation as function of the binding constant for different CO partial pressures. A total carrier concentration of 0.1 M is assumed for the selectivity calculations, but higher carrier concentrations will increase the selectivity even further.

Both the selectivity and capacity utilisation show an increase with binding constant, K_{CO}. The selectivity and capacity utilisation increases linearly with K_{CO} at lower CO partial pressures ($K_{CO}H_{CO}P_{CO} \ll 1$), while at higher partial pressures of CO the carrier material will go to saturation resulting in a diminished increase in selectivity and capacity utilisation with K_{CO}. Selectivity of commercial adsorbents for CO/N_2 separation range between 20–25,[4] highlighting the potential of $K_{CO} > 100$ M^{-1}.

Capacity utilisation in electrochemical separation is directly related to the energy consumption as the energy required to activate the carrier ($Cu^{2+} \rightarrow Cu^+$) will only result in this fraction of the carrier capturing a CO. Thus, the lower capacity utilisation at lower K_{CO} will result in lower energy efficiencies. Therefore, finding a carrier material with high binding affinity for the target gas will increase both selectivity and energy consumption of the separation process.

Determination of the CO binding constant from the cyclic voltammetry shift

The binding constant of ligands can be obtained from electrochemical techniques through the shift of the half-wave potential ($E_{1/2}$) of the redox couple.[10,16–18] The potential of a redox couple is described through the Nernst equation and depends on the formal standard potential ($E^{0'}$) and the concentrations of the oxidized and reduced species of the redox couple (eqn (4)).

$$E = E^{0'} + \frac{RT}{nF}\ln\left(\frac{[Cu^{2+}]}{[Cu^+]}\right) \quad (4)$$

Here, E is the equilibrium potential (V *vs.* ref), R is the gas constant (8.3145 J mol^{-1} K^{-1}), T is temperature (K), n is the number of electrons involved in the redox reaction, F is the Faraday constant (96 485 C mol^{-1}), and [X] is the concentration of the copper ions (M). In the presence of CO, the copper species can coordinate with CO as described by the equilibrium binding constants (eqn (5) and (6)).

$$K_{CO}^{I} = \frac{[Cu^+CO]}{[Cu^+][CO]} \quad (5)$$

$$K_{CO}^{II} = \frac{[Cu^{2+}CO]}{[Cu^{2+}][CO]} \quad (6)$$

These binding constants between CO and Cu^+ (K_{CO}^{I}) and CO and Cu^{2+} (K_{CO}^{II}) will affect the concentration ratio term in the Nernst equation (Fig. 2), as described in SI-2. Therefore, the expected shift with CO concentration as function of the CO binding constants can be expressed by eqn (7).

$$\Delta E = E^{CO} - E^{N_2} = \frac{RT}{nF}\ln\left(\frac{1 + K_{CO}^{I}[CO]}{1 + K_{CO}^{II}[CO]}\right) \quad (7)$$

Assuming the binding of CO to Cu^{2+} is negligible ($K_{CO}^{II}[CO] \ll 1$), the equation can be reduced to eqn (8).[13,14,16] This relation has been used for similar systems to determine the binding constant of a gas molecule to a redox-active carrier from cyclic voltammetry measurements.[19–21]

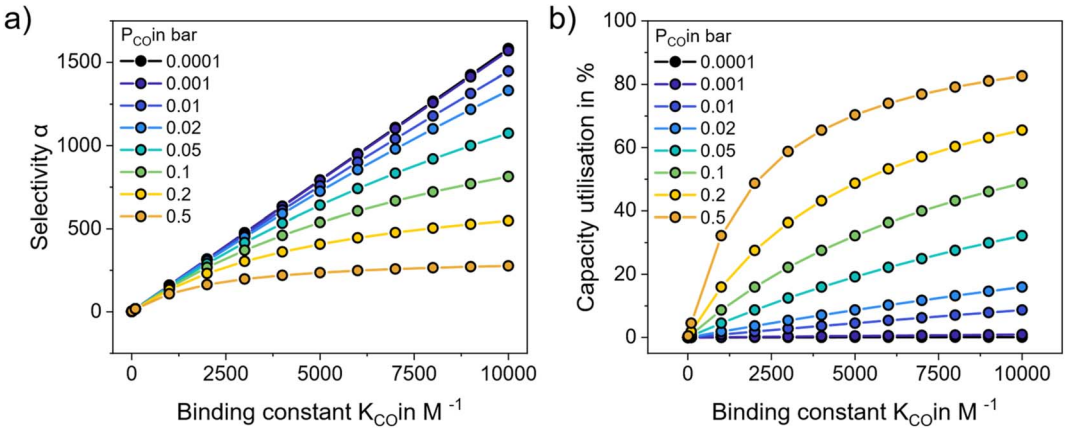

Fig. 1 How the binding constant (K_{CO}) translates to (a) selectivity and (b) capacity utilisation at equilibrium for different partial pressures of CO, following the equilibrium equations. The total pressure is set at 1 bar with N_2 balancing the total pressure and the total carrier concentration is set at 0.1 M for the selectivity estimation.

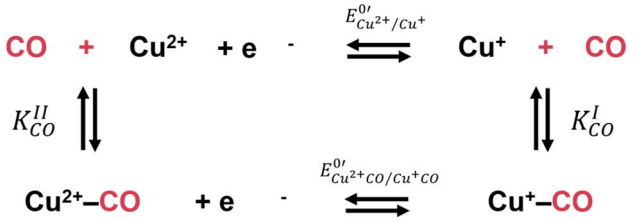

Fig. 2 Binding of CO to Cu^+ and/or Cu^{2+} will shift the Nernst equilibrium of the redox couple and depends on the binding constants (K^I_{CO} and K^{II}_{CO}). Derivation of change in standard potential in SI-2.

$$\Delta E = \frac{RT}{nF}\ln\left(1 + K^{\mathrm{I}}_{\mathrm{CO}}[\mathrm{CO}]\right) \quad (8)$$

From now we will assume the binding to Cu^{2+} to be negligible and use K_{CO} to describe the binding between Cu^+ and CO.

Methods section

Materials

CuCl (99%), $CuCl_2 \cdot 2H_2O$ (99%), K_2SO_4 (99%), KCl (99%), $MgCl_2$ (99%) and HCl (37%) were purchased from Thermo Fisher Scientific. $CuSO_4 \cdot 5H_2O$ (99%) was purchased from Alfa Aesar, $CaCl_2 \cdot 2H_2O$ (99%) was purchased from Sigma Aldrich and NaCl was purchased from Avantor. The electrolyte solutions were prepared with demineralized water and the required salts. The copper salts were added as the final preparation step to minimize exposure to air before the measurement. 50 vol% CO in N_2 was purchased from Linde and used to create CO and N_2 mix gases at different CO concentrations through dilution with N_2 gas. The electrode materials were a glassy carbon rod working electrode (WE) (Ø = 2 mm, type 1, Thermo Scientific), a platinum wire counter electrode (CE) (Ø = 0.3 mm, 99.9%, Thermo Scientific) and Ag/AgCl micro reference electrodes (RE) (LF-1-45, Alvatek) for cyclic voltammetry measurements. A glassy carbon foam (d = 6.35 mm, porosity = 96.5, Goodfellow) was used as WE and CE for capture and release experiments.

Cyclic voltammetry

Cyclic voltammetry (CV) scans were performed at different scan rates (25, 50, 100, 200, 400 mV s^{-1}) using an IviumStat2.h. The measurements were performed in an airtight cell with a gas inlet and outlet to allow for gas flow through the electrolyte (Fig. 3a). The gas flow was controlled with mass flow controllers (MFC, Bronckhorst) and ranged between 0 to 50 vol% CO in N_2 at flow rate of 2 mLn min^{-1}. The solution was sparged with the gas at a certain CO concentration for 2.5 hours before starting the CV measurements. The CV scans were compensated for ohmic drop, using the resistance obtained from electrochemical impedance spectroscopy (EIS) measurements (frequency: 1000–1 Hz, amplitude: 0.01 V, potential: solution's open circuit potential). The experiments were performed at room temperature (±20 °C) and a gas pressure of about 1.1 bar. The actual gas pressure was recorded and used to calculate the CO partial pressure.

Capture and release – H-cell

Capture and release of CO were performed at room temperature (±20 °C) and a gas pressure of about 1.1 bar in an airtight H-cell (Fig. 3b). The cell consists of a working and a counter compartment separated by an anion exchange membrane (AEM, Selemion). Both compartments contain 30 mL of the same electrolyte solution with carrier as specified per experiment. The working compartment has a glassy carbon foam WE, an Ag/AgCl RE and a gas inlet and outlet. The electrolyte in the working compartment was sparged with gas with a flow rate of 10 mLn min^{-1} and a composition of 5 vol% CO in N_2 using mass flow controllers. The flow rate of the gas leaving the compartment was measured with a mass flow meter (MFM, Bronkhorst) and the gas composition was quantified with a 990 MicroGC (Agilent, COX and Molsieve 5A Column, TCD detector) and a mass spectrometer (MS, Pfeiffer Vacuum T100 gas

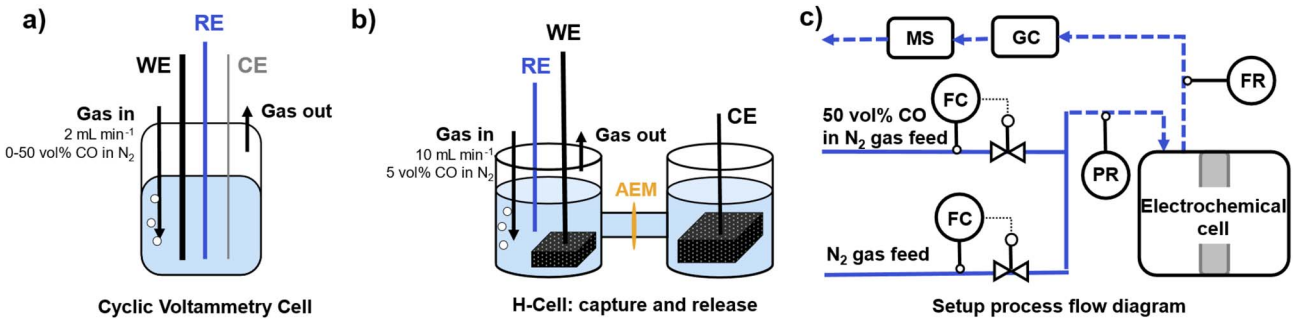

Fig. 3 Schematic illustrations of (a) the cell used for cyclic voltammetry measurements, (b) the H-cell used for capture and release experiments, and (c) a process flow diagram of the setup.

analyser). The counter compartment only required a glassy carbon foam counter electrode to allow the counter reaction. An IviumStat2.h was used to apply a constant potential to the working electrode. A reductive potential was used to reduce the copper to Cu^{+} and induce capture of CO, while an oxidative potential is applied to oxidise the copper to Cu^{2+} resulting in release of previously captured CO.

The potentials for the reduction (capture) and oxidation (release) cycle were chosen using two different methods. The first method used the same reduction and oxidation potentials *vs.* the RE for each electrolyte solution, 0 V and 0.7 V *vs.* Ag/AgCl, respectively. In the second method, the reduction and oxidation potential were determined from the open circuit potential (OCP) at equimolar $[Cu^{+}]$ and $[Cu^{2+}]$. To achieve equimolar $[Cu^{+}]$ and $[Cu^{2+}]$, the solution was first oxidised for a long time to convert all copper species to Cu^{2+}. Then a reduction potential was applied until the amount of charge transferred matches conversion of half of the Cu^{2+} to Cu^{+} (28.9C), after which the OCP was measured. The reduction potential for the capture half-cycles were then set to the initially measured OCP – 0.35 V and the release was initiated by increasing the potential in steps of 5 hours.

Before starting the capture and release experiment, the working solution was oxidised to the low affinity state (Cu^{2+}) under N_2 environment. After 30 minutes, the CO containing gas is introduced to flush the lines and solution for 60 minutes while still at the oxidative potential. After this, capture of CO is initiated by reduction of the carrier to its high affinity state (Cu^{+}). We allowed the system to capture CO for 5+ hours, assuming it to be sufficient to reach capacity saturation. Then, the CO release was achieved through oxidation for 5+ hours.

DFT calculations

All DFT calculations were performed using ORCA 6.0 with the PBE0 hybrid-GGA functional and Karlsruhe def2 basis sets.[22–25] Dispersion was taken into account using Grimme's D3 correction with Becke–Johnson damping.[26,27] Implicit solvation with pure water was modelled using the Solvation Model based on Density (SMD).[28] Calculation times were shortened using the RIJ-COSX approximation using the def2/J auxiliary basis set.[29,30]

Initial geometries for all complexes were made in Avogadro2.[31] We considered Cu^{+} with 0 to 4 ligands of either CO, Cl^{-}, or a combination of both. Geometry optimizations were performed using the def2-SVP basis set, while the single point calculations were performed using the def2-TZVPP basis set for increased accuracy. Frequency calculations were performed on all optimized structures to obtain thermochemistry data and to confirm the optimization to a (local) minimum. Binding enthalpies and Gibbs free energy differences were calculated by comparing the energy of the complex with ligand, with that of the complex without this ligand, and the non-bonded ligand at the conformations with the lowest energies. To gain quantitative insight into the effect of Cl^{-} ligands and the geometry on σ-donation and π-backdonation interactions, the orbital energy portion of the binding energy was decomposed using Extended Transition State Natural Orbitals for Chemical Valence (ETS-NOCV) analysis in Multiwfn 3.8.[32–37]

Minteq for copper chloride solution composition

To predict the copper chloride species distribution, we used Visual Minteq software. Due to high salt concentrations in our simulated solution, we used the Specific ion Interaction Theory (SIT) model for activity correction. Note that at very high concentrations (>1 M) this model can still be less accurate than for example Pitzer-based models. The temperature was set at 25 °C and the pH was calculated from mass and charge balance.

UV/vis spectroscopy

UV/vis spectroscopy was performed on CuCl (0.5 mM) or $CuCl_2$ (0.5 mM) solutions for different electrolyte compositions. The solution's absorbance was measured inside quartz cuvettes and at a wavelength range of 400 to 200 nm. To minimise the exposure to air, the solution was immediately measured after preparation.

Results & discussion

The expected effect of chloride ions on CO binding

Chloride ions (Cl^{-}) are essential to stabilise Cu^{+} species and prevent dissociation in Cu^{0} and Cu^{2+} species. Depending on the free chloride concentration, different copper chloride complexes will form. The possible complexes for Cu^{2+} include Cu^{2+}, $CuCl^{+}$, $CuCl_2$, $CuCl_3^{-}$, and $CuCl_4^{2-}$ and for Cu^{+} they

Table 1 Gibbs free energy change in kJ mol^{-1} from coordination of 1st to 4th CO ligands to different Cu^+ chloride complexes

	1st CO	2nd CO	3rd CO	4th CO
Cu^+	−94	−83	−36	−21
CuCl	−106	−11	−3	
$CuCl_2^-$	−7	8		
$CuCl_3^{2-}$	−2			

include Cu^+, CuCl, $CuCl_2^-$, and $CuCl_3^{2-}$.[38] Besides stabilisation of the 1+ oxidation state, literature suggests that the Cl^- ions enforce π-backbonding from the Cu^+ to the π-acid CO ligand through electron donation.[39,40] Therefore, we expected that the addition of Cl^- ligands to the Cu^+ complex increases the CO binding affinity. However, our DFT calculations show a different trend (Table 1). Cu^{2+} species are expected to have negligible CO affinity ($K_{CO}^{II} < 1$) compared to Cu^+ species.[13]

All cuprous chloride complexes have a binding affinity for CO as illustrated by the negative change in Gibbs free energy (except $CuCl_2^-$–CO with a second CO). For the effect of chloride ligands, only CuCl shows a more negative ΔG for binding of a single CO compared to Cu^+. In any other case, the addition of a Cl^- ligand lowers the affinity to bind CO.

Separating the different contributions to the ΔG through orbital analysis confirms that π-backbonding does increase with increasing Cl^- coordination, but other effects such as geometric and electrostatic effects dominate the overall affinity (SI-4).[16] The single chloride ligand in CuCl allows for the coordination of a CO without reorganisation of the ligands and the maintained linear geometry facilitates a linear path for the electron pushing of the chloride ligand to the π-accepting CO ligand (Fig. 4). This results in a more favourable CO binding for CuCl compared to Cu^+. For higher chloride complexes such as $CuCl_2^-$, the coordination of a CO requires reorganisation from a linear geometry to a trigonal geometry, introducing an energy cost. Additionally, the electron donation from the two chloride ligands is at an angle, which gives less of an energy gain compared to the linear single chloride ligand. Thus, the DFT calculations show that cuprous chloride complexes bind CO, with CuCl having the strongest binding to CO and any more chloride ligands resulting in weaker binding.

Electrolyte composition and copper chloride complexes

The DFT calculations have shown a difference in binding affinity of the various copper chloride species, meaning that the actual binding affinity of a copper chloride solution will depend on the presence and contribution of these different species. It is expected that the copper chloride species contribution changes with total chloride concentration, which is also reflected in a visible colour change of the solution from light blue to green upon increase of the Cl^- concentration (Fig. S6). We calculate the expected composition of copper chloride solutions with Visual Minteq as function of the chloride concentration and for different cations (Fig. 5).

The species with the strongest CO binding (Cu^+ and CuCl) are only present in very low amounts (<0.05% and <4% respectively) at Cl^- concentration > 0.1 M and, as expected, the contribution of the higher coordinated cuprous chloride species increases with chloride concentration (Fig. 5a and b). Combined with the estimated binding affinity of the different cuprous chloride species from DFT, this would mean that the binding affinity of a copper chloride solution will decrease with chloride concentration. The cation type does affect the composition, especially at the higher chloride concentrations (Fig. 5c and d). This can largely be attributed to the different Cl^- activity of the electrolytes (SI-6) caused by the different solution environment and interactions with the counterion.[41,42] The DFT calculations and expected compositions of the electrolyte suggest that the CO binding could be strongest when the lower coordinated CuCl species could be promoted.

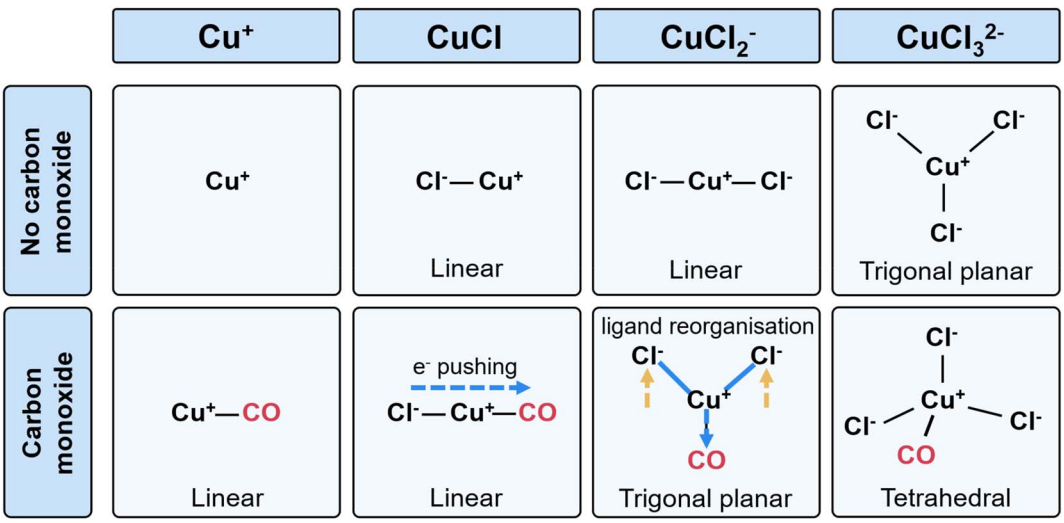

Fig. 4 Geometries of copper(I) chloride complexes with and without CO coordination. The blue arrows show electron pushing for π-backbonding between Cu^+ and CO and the orange arrows show the reorganisation of ligand by introduction of the CO ligand.

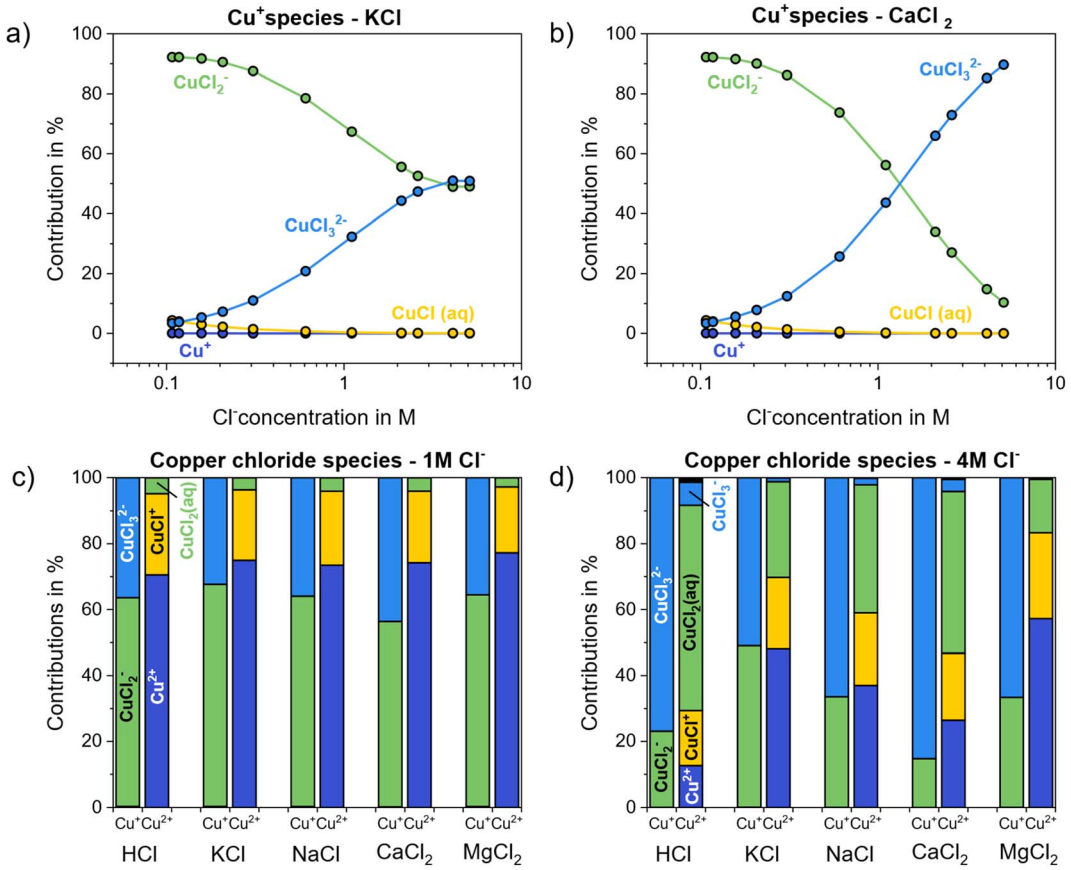

Fig. 5 Copper chloride species contributions calculated by Visual Minteq. The effect of the total Cl^- concentration on the Cu^+ chloride species for (a) KCl and (b) $CaCl_2$ electrolytes with 0.1 M HCl. The total Cl^- concentration of the *x*-axis is the sum of the Cl^- ions from KCl/$CaCl_2$, HCl and copper chlorides. The copper chloride species for different chloride salts at a Cl^- concentration of (c) 1 M and (d) 4 M, with additionally 0.1 M HCl, resulting in a total Cl^- concentration of 1.1 M and 4.1 M respectively. For all simulations the copper concentration is 2.5 mM Cu^+ and 2.5 mM Cu^{2+}.

Binding constant for different electrolyte compositions

With cyclic voltammetry measurements, we can measure the actual CO binding affinity of a solution and estimate the effect of the electrolyte composition. Eqn (8) describes how CO coordination to Cu^+ will shift the redox couple's potential as a function of the CO concentration. To determine the CO binding constant for different copper chloride solutions, we measure this shift from the oxidation peak at different CO

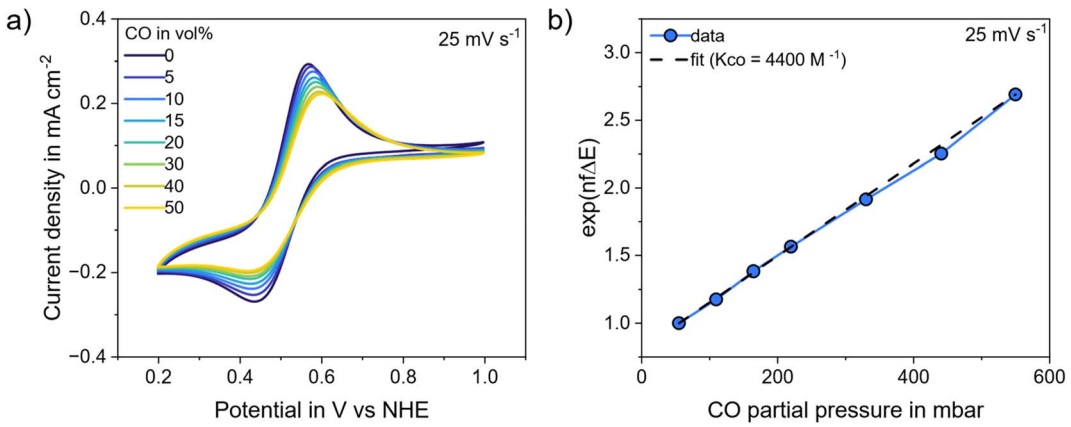

Fig. 6 (a) Cyclic voltammetry measurement of 2.5 mM CuCl and 2.5 mM $CuCl_2$ in 1.25 M $CaCl_2$ 0.03 M HCl electrolyte at 25 mV s^{-1}. The gas flow rate is 2 mL min^{-1} with different CO concentrations, and the remaining gas is N_2. (b) The exponent of the potential shift in the CV measurement plotted against the partial pressure of CO and the fit with eqn (S34) to estimate the binding constant (here 4400 M^{-1}) by minimising the mean average error.

partial pressures. Using this relation, worked out in SI-3 for CV processing, we fit the data and estimate the CO binding constant of the carrier solution. An example of a CV measurement and the fitting of the data is presented in Fig. 6.

Fig. 6a shows an anodic shift of the redox couple with CO concentration, indicating a stronger binding affinity to the carrier's lower oxidation state (Cu^+). This shift is more prominent in the oxidation peak than the reduction peak, which could be caused by slow CO coordination kinetics. That is, the CO coordination during reduction is too slow to shift the reaction equilibrium towards reduction of Cu^{2+} to Cu^+CO, while the Cu^+ had more time to interact with CO when it gets oxidised as Cu^+CO to Cu^{2+} and CO. Fitting the shift of the oxidation peak with the CO partial pressure gives an estimated CO binding constant of 4400 M^{-1} (Fig. 6b). Additionally, the peak currents decrease with CO concentration which could be caused by slower kinetics of the redox reaction with CO.[13] For example, the oxidation of Cu^+CO might be slow because it requires ligand reorganisation or CO adsorption on the electrode surface might affect the reactions kinetics.[13,43]

The estimated binding constant for the different copper chloride solutions are combined in Fig. 7. For comparison, literature reports a binding constant of 1600 M^{-1} for a 1 M KCl and 0.1 M HCl electrolyte, which compares well to our experimentally obtained value of 1800 $\pm$ 600 M.[13] We also observe that the binding constant for most other compositions is substantially higher, even up to 6000 M^{-1}.

Most electrolytes show a decrease in binding constant with Cl^- concentration or activity, except for KCl. The decrease in binding affinity with Cl^- concentration was indeed predicted from our DFT calculations. Of all electrolytes, KCl is the only electrolyte that breaks this trend, and even shows a slight increase in binding constant when increasing its concentration from 1 M to 2.5 or 4 M. KCl also shows the smallest change in copper species distribution between 1 and 4 M Cl^- concentration (Fig. 5): the $CuCl_2^-$ decreases from 67% to 49%, while for $CaCl_2$ it decreases from 56% to 15%. This might contribute to the different trend of KCl with Cl^- concentration, but it does not explain the slight increase in binding constant with Cl^- concentration. Still, the binding constant of the carrier solution with KCl electrolyte at higher chloride concentration remains lower than that of the $CaCl_2$ electrolyte, making the $CaCl_2$ the better electrolyte for electrochemical CO separation.

With increasing Cl^- concentration, the overall ionic strength also increases. This can introduce salting-out effects,[44,45] which might affect the CO solubility and thus the estimated binding constant. Control experiments with different Cl^- concentration at the same ionic strength confirm the decrease in binding constant with Cl^- concentration (SI-9).

To understand the difference between electrolytes we correlated the binding constants with the different copper chloride species distributions, however, they do not seem to explain the observed differences (SI-10). The copper species distribution generally follows the Cl^- activity, and the binding constant plotted against the Cl^- activity or copper species still shows differences between electrolyte types (Fig. S17). The total Cl^- concentration, or the Cl^- activity (Fig. 7b), seems a better predictor for the binding constant than the cuprous chloride complex speciation.

We further explored the influence of the cations on the Cu^+–CO interaction from a theoretical framework. Depending on the Cl^- concentration, we roughly see an increase in CO binding from KCl, NaCl < HCl < $MgCl_2$ < $CaCl_2$. For a (non-electrochemical) CO absorption system using copper chloride salts, an increase in CO uptake was observed from KCl < HCl < $MgCl_2$ and Johnsen *et al.* showed that the addition of Lewis acids increases the CO coordination to a dinuclear Cu^+ complex.[46,47] It is suggested that Lewis acids stabilise the coordinated CO through interaction with the oxygen atom.[47] With π-backbonding strengthening the coordination between CO and Cu^+, an increasingly good π-acceptor will complex stronger with Cu^+.[10] Interaction between the oxygen of CO and the Lewis acid could increase the CO's π-acidity by withdrawing electron density from the carbon. The Lewis acidity and/or charge

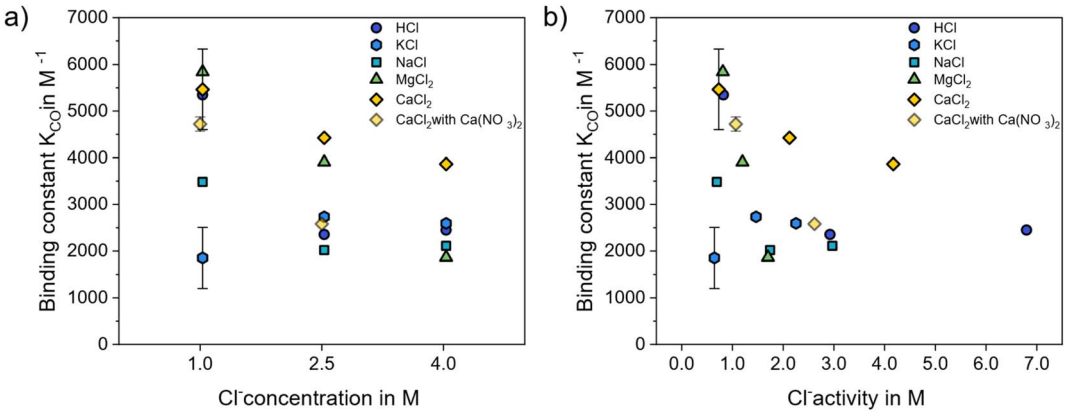

Fig. 7 CO binding constant obtained from CV measurements (at 25 mV s^{-1}) for different electrolyte compositions plotted against (a) the Cl^- concentration and (b) the Cl^- activity (obtained from Minteq). The faint $CaCl_2$ with $Ca(NO_3)_2$ data points represent a control where the ionic strength is kept constant at 6 M by the additions of $Ca(NO_3)_2$ salt. The KCl and $CaCl_2$ data points with an error bar are the average of 3 measurement series and the $CaCl_2$ with $Ca(NO_3)_2$ with error bar is the average of 2 measurement series. Other compositions without an error bar are based on a single measurement.

density of the cation increase with charge and decrease with volume of the cation ($K^+ < Na^+ < Ca^{2+} < Mg^{2+} < H^+$).[48] It seems that the Lewis acidity of the cations can partly explain the differences in binding constant. However, a quantitative relation between charge density, Cl^- activity and/or cation activity has not been found.

The Cl^- concentrations plotted in Fig. 7 (1 to 4 M) allowed for K_{CO} determination through the shift of the oxidation peak potential with CO concentration. We also attempted to measure the binding constant at even lower Cl^- concentrations, as it is expected to have stronger CO binding, but the seemingly appearing of a second peak complicates the system (SI-11). This could imply that perhaps at all Cl^- concentrations the change of the CV with CO is not necessarily a shift of the peak, but perhaps the splitting of the Cu^+ oxidation into two nearby peaks (SI-12). Each copper chloride complex is expected to have a unique redox potential, depending on Cl^- and CO coordination. The overall Cu^+/Cu^{2+} redox potential should be a weighted average in the case of equilibration between the species.[38]

Stability window for different electrolyte solutions

The chloride concentration will not only affect the CO binding affinity but also plays a role for the stability of the activated carrier (Cu^+). For practical application, the carrier concentration and its stability will be important to maintain a high CO capacity of the electrochemical separation process. Fig. 8 presents the effect of Cl^- concentration and electrolyte on the Cu^0/Cu^+ and Cu^+/Cu^{2+} redox potentials.

Fig. 8a and b show the CVs and half-wave potentials ($E_{1/2}$) of the electrolyte solution compositions used to determine K_{CO} (for $CaCl_2$, KCl and HCl). The peaks at more negative potentials represent the Cu^0/Cu^+ redox couple and the peaks at more positive potentials represent the Cu^+/Cu^{2+} redox couple. Clearly, increased Cl^- concentration results in a larger separation of the Cu^0/Cu^+ and Cu^+/Cu^{2+} redox potentials. This increased separation of the two redox reactions allows for the formation of Cu^+ and ensures a larger potential window for stabilised Cu^+ species, which are the active species for CO capture. There is no large difference between different cations, except for a slightly more negative Cu^0/Cu^+ potential for HCl (Fig. 8b). This confirms that the Cu^+ stability window is determined by the Cl^- concentration and hardly affected by the cation type.

To rule out the effect of ionic strength and electrical conductivity, we performed the same exercise with supporting electrolyte (K_2SO_4) to vary the Cl^-/Cu ratio while maintaining the ionic strength and conductivity (Fig. 8c and d). If no Cl^- is

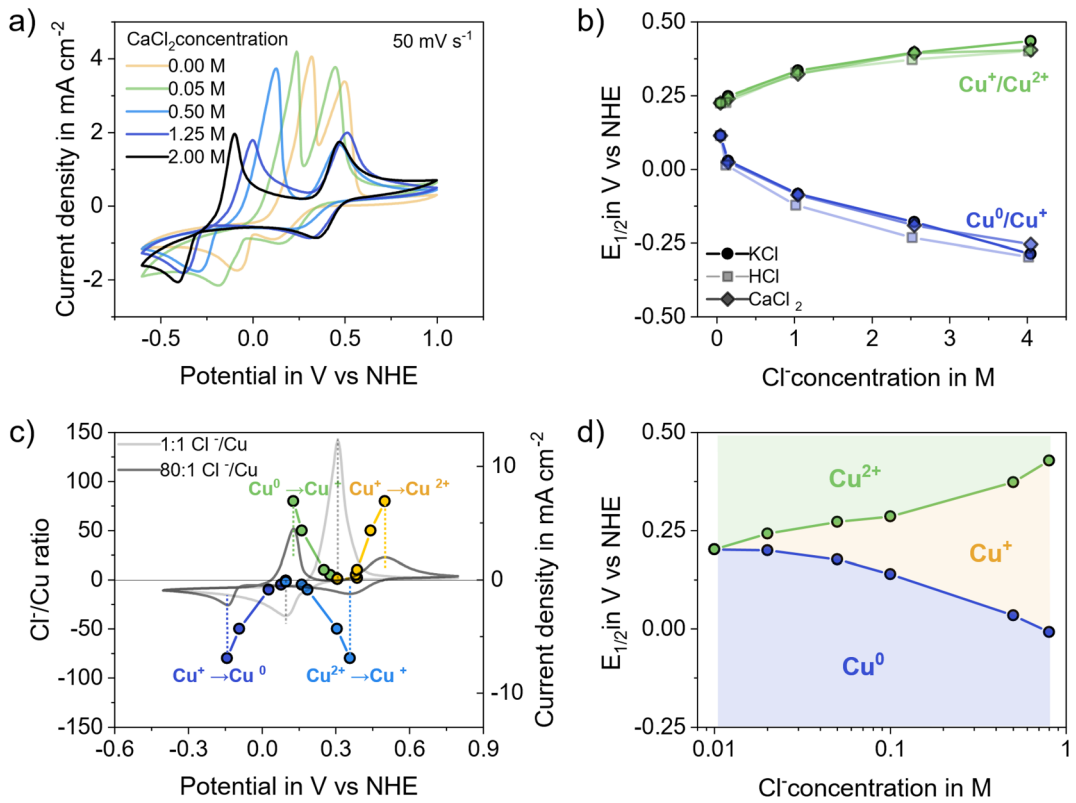

Fig. 8 The effect of Cl^- ions on the electrochemical Cu^+ potential window (under N_2 atmosphere). (a) Cyclic voltammetry curves at a scan rate of 50 mV s^{-1} for the different $CaCl_2$ solution compositions used for the K_{CO} determination. (b) Half-wave potential of the Cu^0/Cu^+ and Cu^+/Cu^{2+} reactions obtained from the CV curves at the different Cl^- concentrations for KCl, $CaCl_2$ and HCl electrolytes. The solutions for (a and b) consist of 10 mM copper ions, 0.03 M HCl, and the electrolyte at the different Cl^- concentrations (0, 0.1, 1.0, 2.5 and 4 M). (c) Peak potentials of the copper oxidation and reduction reactions as a function of the Cl^-/Cu ratio (left y-axis) and in the background, CV curves for 1 : 1 and 80 : 1 Cl^-/Cu ratio (right y-axis). (d) Copper oxidation state diagram as a function of potential and Cl^- concentration at log scale. The solutions for (c and d) consist of 10 mM $CuSO_4$ and different concentrations of KCl and K_2SO_4 to vary the Cl^- concentration while keeping the conductivity similar (SI-13).

present, only one oxidation and reduction peak is observed, corresponding to the two-electron Cu^0/Cu^{2+} redox reaction (Fig. 8c). With increasing Cl^- concentration, these peaks separate into two one-electron redox couples (Cu^0/Cu^+ and Cu^+/Cu^{2+}) and allow for a stable Cu^+ potential window. This is translated into a copper oxidations state diagram in Fig. 8d.

The shift of the redox couples with Cl^- concentration can be explained by the different copper chloride species at those concentrations ($CuCl_2^-$, $CuCl_3^{2-}$, Cu^{2+}, $CuCl^+$ *etc.*). Each of the copper species will have a different redox potential for Cu^0/Cu^+ and Cu^+/Cu^{2+} redox reactions and the observed redox potential will be a weighted average of the redox couples.[38,49]

As stability of Cu^+ at higher copper concentrations is important for application, we need to distinguish whether absolute Cl^- concentration or Cl^-/Cu ratio is determining for the stability. At high Cl^- concentrations, the species distributions obtained from Visual Minteq show minimal effect of total copper concentration (Fig. S11). CV measurements with a 10 times higher copper concentration show a small shift for the Cu^0/Cu^+ peak towards more positive potentials (Fig. S21), which would decrease the Cu^+ stability window. However, compared to the dilute copper solutions in Fig. 8b, the Cu^+ stability window is more similar for the same Cl^- concentration than the same Cl^-/Cu ratio. Thus, it is expected to have a slight decrease in Cu^+ stability window at higher copper concentrations, but the absolute Cl^- concentration seems to be decisive rather than the Cl^-/Cu ratio.[50] This would allow the increase of carrier concentration at high Cl^- concentration.

Capture and release of CO

To verify the effect of the binding constant in a cyclic process, capture and release experiments were performed for three of the different binding constants (1 M KCl with 1800 M^{-1}, 1 M HCl with 5300 M^{-1}, and 0.5 M $CaCl_2$ with 5500 M^{-1}). The CO concentration profiles are presented in Fig. 9.

Upon reduction of the carrier material, the CO profile clearly shows a decrease in CO concentration due to binding of CO to the Cu^+ carrier (Fig. 9a). Subsequently, an increase in CO concentration upon oxidation to Cu^{2+} indicates release of the previously captured CO (Fig. 9b). In both cases, the CO concentration slowly returns to the baseline as the carrier solution reaches saturation. A higher binding constant should naturally result in more capture of CO through a higher CO capacity. The CV determined and experimental values are presented in Table 2. Method 1 represents an experiment with the same constant potential relative to the reference electrode for all carrier solutions. Similar results are obtained when the potential is dependent on the open circuit potential (Method 2, see SI-16).

Table 2 Theoretical and experimental values for CO capacity and carrier utilisation of a 20 mM copper chloride solution. Method 1 uses the same reduction and oxidation potentials for each carrier solution (0 and 0.7 V respectively) and Method 2 uses the same change in potential from the measured OCP (OCP − 0.35 V for reduction)

		1.0 M KCl	1.0 M HCl	0.5 M $CaCl_2$
CV determined	K_{CO} (M^{-1})	1850	5350	5500
	CO capacity (mL)	1.2	2.9	3.0
	Cu utilisation (%)	9	22	22
Method 1	CO capacity (mL)	1.23	1.52	1.43
	Cu utilisation (%)	9.2	11.3	10.6

Here we observe that the expected increase in CO capture efficiency for electrolytes with higher binding constants does not materialize. Only the captured amount of CO for 1 M KCl agrees well with the estimated binding constant for both methods (Table 2). Although HCl and $CaCl_2$ have a higher CO capacity than KCl, the difference is substantially smaller than what the estimated K_{CO} predicts. With all CO capacities being similar, it seems something else is determining the measured CO capacity in these experiments or counteract the benefit of a higher binding constant.

Although we are not sure why the CO separation in cyclic mode is only mildly dependent on the binding constant, we

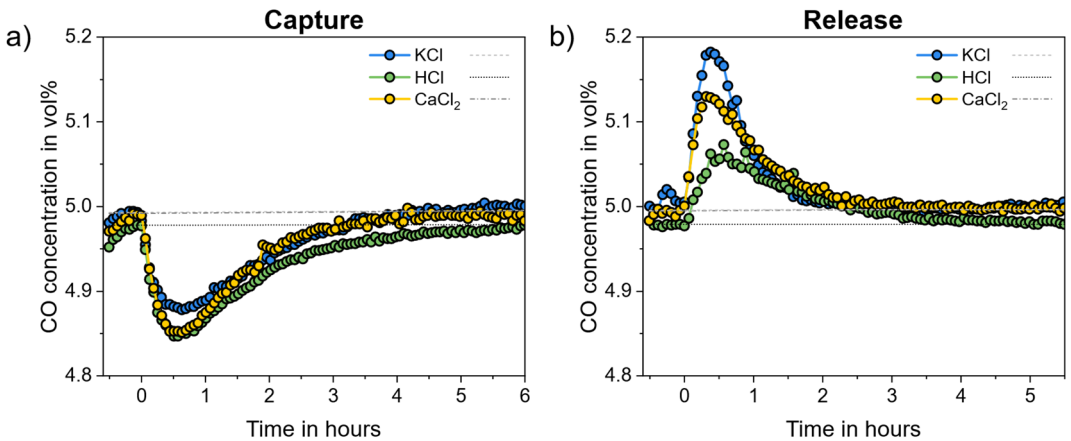

Fig. 9 CO concentration profiles during (a) capture and (b) release of CO for three electrolyte solutions: 1 M KCl, 1 M HCl, 0.5 M $CaCl_2$ with 0.03 M HCl, 10 mM CuCl and 10 mM $CuCl_2$. The grey dotted lines represent the estimated baselines from GC values before and after the experiment. The $t = 0$ represents the start of reduction in (a) and the start of oxidation in (b). These are the results for experiments using Method 1.

should consider that the nature of the electrolyte can affect other gas interaction properties.[44,51,52] However, salting-out effects, although stronger for divalent cations than for monovalent cations,[43,44] cannot explain the deviation of the capture capacity from the estimated K_{CO}. If anything, salting-out effects during the CV measurements could underestimate the CO binding constant.

The different copper concentrations for the CV and absorption measurements or the possible formation of other Cu^+–CO complexes do not seem to explain the discrepancy between the estimated K_{CO} and measured CO capacity either (SI-16). Refitting for $(Cu^+)_2CO$ or $Cu^+(CO)_2$ would give a too high or too low CO capacity compared to our results, respectively. Furthermore, our CV measurements do not support the formation of $(Cu^+)_2CO$ or $Cu^+(CO)_2$ but suggest the binding of a single terminal CO (Cu^+CO) (SI-3).

Something that does play a role in the discrepancy between the expected and measured Cu utilization and CO capacity is the inaccuracy in baseline determination. The slow capture (over 5+ hours) and thus small CO concentration change measured in the GC, makes that the set baseline strongly affects the calculated accumulated amount. The baseline is set to the best of our estimation from the GC values before and after the experiment when feeding the CO containing gas without capture or release. However, we note a high sensitivity to the set baseline with a change of 0.01 vol% for the CO baseline giving an increase in captured CO of 30–40%.

Furthermore, the slow capture and release are partly due to poor mass transport inside the H-cell. Moving to an electrochemical flow cell and separate absorption units (*e.g.* membrane contactors) can improve the CO sorption and desorption rates through increased carrier activation (current density) and gas–liquid contact. The high binding constants of the electro-active carrier could offer competitive selectivity to commercial CO/N_2 adsorbents[4] and high capacity when fully utilised.

Conclusion

Finding an electro-active carrier with a high binding constant to CO could offer a selective and energy-efficient solution to separate CO from N_2. Copper chlorides have demonstrated high binding affinity to CO, but further exploration and understanding of the binding interaction could lead to improvements in separation performance. We have investigated the effect of electrolyte compositions on the CO binding affinity of an electro-active copper chloride carrier. Cyclic voltammetry measurements estimate the binding constant from the potential shift induced by CO coordination. A comparison of different electrolyte types (KCl, NaCl, HCl, $CaCl_2$, and $MgCl_2$) and Cl^- concentrations (1, 2.5, and 4 M), resulted in different binding constants ranging from 1800 to 6000 M^{-1}. Generally, the binding constant decreases with increasing Cl^- concentration. This is also supported by computational data as the higher-coordinated chloride complexes have weaker binding with CO due to geometrical effects. We observe a difference in binding constant among electrolyte types, which partly follows the Lewis acidity of the cations. We propose that interactions between the cation and the O of the CO ligand can strengthen the π-back-bonding between Cu^+ and CO. The CO capture capacity of KCl agrees with the estimated binding constant, but the other two electrolytes with higher binding constant (HCl, $CaCl_2$) do not show the expected increase in CO capture. Besides binding constant, carrier concentration and stability are determining for the CO separation performance, such as selectivity. High Cl^- concentrations will be necessary to stabilise Cu^+ and allow high carrier concentrations to increase the CO capacity and selectivity of the system. This reveals a trade-off between the CO binding constant and stability of the copper chloride carrier with the Cl^- concentration. Further research into the carrier material could explore other ligands to stabilise Cu^+ while maintaining its CO binding affinity (*e.g.* acetonitrile, ammonia or cyclam). All in all, to develop an efficient electrochemical separation method for CO/N_2, the carrier and electrolyte selection requires considerations of the binding constant, stability and carrier solubility.

Conflicts of interest

There are no conflicts to declare.

Data availability

(1) The data for all figures and tables are included in excel files. (2) The DFT data for the NOCV analysis for the three complexes in text files. (3) The raw data sets of the CV measurements for K_{CO} determination as Ivium (ASCI type) files are available at Zenodo, DOI: https://doi.org/10.5281/zenodo.18549588 at https://zenodo.org/records/18549588. In addition, the methods for processing the data have been included as part of the supplementary information (SI). Supplementary information: derivations for the CO binding constant, selectivity and carrier utilisation; DFT orbital analysis data; UV/vis spectra and pictures of the copper chloride solutions; additional data for the copper chloride distributions from Minteq; additional CV measurements, including at lower chloride concentrations; comparison of the CO binding constant data with the copper chloride species distribution; CV peak shape analysis; additional discussion on the capture and release experiments including Method 2. See DOI: https://doi.org/10.1039/d6ta01538g.

Acknowledgements

This publication is part of Target 4 of the TTW Perspectief research programme ReCoVR: Recovery and Circularity of Valuable Resources (P19-20), which is (partly) financed by the Dutch Research Council (NWO). This work used the Dutch National e-Infrastructure with the support of the SURF Cooperative using grant no. EINF-11304.

References

1 S. Santos, *et al.*, *Iron and Steel CCS Study (Techno-economics Integrated Steel Mill)*, IEAGHG, 2013.
2 E. Kennedy, *et al.*, *CORESYM: Carbon-Monoxide Re-use through Industrial Symbiosis between Steel and Chemical Industries*, Metabolic, 2017.
3 J. James, L. E. Lücking, H. van Dijk and J. Boon, Review of technologies for carbon monoxide recovery from nitrogen-containing industrial streams, *Frontiers in Chemical Engineering*, 2023, **5**, 1066091.
4 X. Ma, *et al.*, Carbon monoxide separation: past, present and future, *Chem. Soc. Rev.*, 2023, **52**, 3741–3777.
5 J. Arvola, J. Harkonen, M. Mottonen, H. Haapasalo and P. Tervonen, Combining steel and chemical production to reduce CO_2 emissions, *Low Carbon Econ.*, 2011, **2**(3), 115–122.
6 A. Nowaczyk, M. Kowalska, J. Nowaczyk and G. Grześk, Carbon monoxide and nitric oxide as examples of the youngest class of transmitters, *Int. J. Mol. Sci.*, 2021, **22**, 6029.
7 G. Frenking, *et al.*, Metal–CO Bonding in Mononuclear Transition Metal Carbonyl Complexes, *JACS Au*, 2021, **1**, 623–645, DOI: 10.1021/jacsau.1c00106.
8 J. Mehara, *et al.*, Binding Interactions in Copper, Silver and Gold π-Complexes, *Chem.–Eur. J.*, 2022, **28**, e202103984, DOI: 10.1002/chem.202103984.
9 E. Lu, *et al.*, Back-bonding between an electron-poor, high-oxidation-state metal and poor π-acceptor ligand in a urnaium(v)-dinitrogen complex, *Nat. Chem.*, 2019, **11**, 806–811.
10 A. W. Addison, M. Carpenter, L. K.-M. Lau and M. Wicholas, Coordination Sphere Flexibility at Copper: Chemistry of a Unipositive Copper(II) Macrocycle, $[Cu(cyclops)]^+$, *Inorg. Chem.*, 1978, **17**, 1545–1552.
11 J. C. Xavier, M. Preiner and W. F. Martin, Something special about CO-dependent CO2 fixation, *FEBS J.*, 2018, **285**, 4181–4195, DOI: 10.1111/febs.14664.
12 C. I. Koopman, J. Albertsma, M. A. van der Veen and D. A. Vermaas, Electrochemically Mediated Separation of Carbon Monoxide Using a Ni-Based Redox Couple, *ACS Energy Lett.*, 2026, **11**(2), 2229–2234, DOI: 10.1021/acsenergylett.5c04138.
13 P. A. Terry, H. J. Walls and R. D. Noble, Electrochemically modulated complexation process for gas removal and concentration, *AIChE J.*, 1995, **41**, 2556–2564.
14 R. R. Gagne and D. M. Ingle, One-electrond-reduced nickel(II)-macrocyclic ligand complexes. Four-coordinate nickel(I) species and nickel(II)-ligand radical species which form paramagnetic, five-coordinate nickel(I) adducts, *Inorg. Chem.*, 1981, **20**, 309–640.
15 X. H. Mu and K. M. Kadish, Oxidative electrochemistry of cobalt tetraphenylporphyrin under a CO atmosphere. Interaction between carbon monoxide and electrogenerated $[(TPP)Co]^+$ in nonbonding media, *Inorg. Chem.*, 1989, **28**, 3743–3747.
16 R. R. Gagne, J. L. Allison and D. M. Ingle, Unusual structural and reactivity types for copper(I). Equilibrium constants for the binding of monodentate ligands to several four-coordinate copper(I) complexes, *Inorg. Chem.*, 1979, **19**, 2767–2774.
17 Y. Meng and A. J. Bard, Measurement of Temperature-Dependent Stability Constants of Cu(I) and Cu(II) Chloride Complexes by Voltammetry at a Pt Ultramicroelectrode, *Anal. Chem.*, 2015, **87**, 3498–3504, DOI: 10.1021/acs.analchem.5b00052.
18 J. Heyrovsky and J. Kuta, *Principles of Polarography*, Academic Press, 1965.
19 J. D. Froehlich and C. P. Kubiak, The homogeneous reduction of CO_2 by $[Ni(cyclam)]^+$: increased catalytic rates with the addition of a CO scavenger, *J. Am. Chem. Soc.*, 2015, **137**, 3565–3573, DOI: 10.1021/ja512575v.
20 X. Li, *et al.*, Redox-tunable isoindigos for electrochemically mediated carbon capture, *Nat. Commun.*, 2024, **15**, 1175, DOI: 10.1038/s41467-024-45410-z.
21 X. Wang, *et al.*, Tuning the Half-Wave Potential and Binding Constant of PAQ Molecules for the Enhanced O2-Tolerant Electrochemical CO2 Capture Process, *ACS Sustain. Chem. Eng.*, 2026, **14**, 3471–3483, DOI: 10.1021/acssuschemeng.5c11680.
22 C. Adamo and V. Barone, Toward reliable density functional methods without adjustable parameters: The PBE0 model, *J. Chem. Phys.*, 1999, **110**, 6158–6170, DOI: 10.1063/1.478522.
23 J. P. Perdew, M. Ernzerhof and K. Burke, Rationale for mixing exact exchange with density functional approximations, *J. Chem. Phys.*, 1996, **105**, 9982–9985, DOI: 10.1063/1.472933.
24 F. Weigend and R. Ahlrichs, Balanced basis sets of split valence, triple zeta valence and quadruple zeta valence quality for H to Rn: Design and assessment of accuracy, *Phys. Chem. Chem. Phys.*, 2005, **7**, 3297–3305, DOI: 10.1039/B508541A.
25 F. Neese, Software update: The ORCA program system - version 6.0, *WIREs Computational Molecular Science*, 2025, **15**, e70019.
26 S. Grimme, J. Antony, S. Ehrlich and H. Krieg, A consistent and accurate ab initio parametrization of density functional dispersion correction (DFT-D) for the 94 elements H-Pu, *J. Chem. Phys.*, 2010, **132**(15), 154104, DOI: 10.1063/1.3382344.
27 S. Grimme, S. Ehrlich and L. Goerigk, Effect of the damping function in dispersion corrected density functional theory, *J. Comput. Chem.*, 2011, **32**, 1456–1465, DOI: 10.1002/jcc.21759.
28 A. V. Marenich, C. J. Cramer and D. G. Truhlar, Universal Solvation Model Based on Solute Electron Density and on a Continuum Model of the Solvent Defined by the Bulk Dielectric Constant and Atomic Surface Tensions, *J. Phys. Chem. B*, 2009, **113**, 6378–6396, DOI: 10.1021/jp810292n.
29 F. Neese, F. Wennmohs, A. Hansen and U. Becker, Efficient, approximate and parallel Hartree–Fock and hybrid DFT calculations. A 'chain-of-spheres' algorithm for the

Hartree–Fock exchange, *Chem. Phys.*, 2009, **356**, 98–109, DOI: 10.1016/j.chemphys.2008.10.036.
30 F. Weigend, Accurate Coulomb-fitting basis sets for H to Rn, *Phys. Chem. Chem. Phys.*, 2006, **8**, 1057–1065, DOI: 10.1039/B515623H.
31 *Avogadro*, https://two.avogadro.cc.
32 T. Ziegler and A. Rauk, On the calculation of bonding energies by the Hartree Fock Slater method, *Theor. Chim. Acta*, 1977, **46**, 1–10, DOI: 10.1007/BF02401406.
33 M. Mitoraj and A. Michalak, Natural orbitals for chemical valence as descriptors of chemical bonding in transition metal complexes, *J. Mol. Model.*, 2007, **13**, 347–355, DOI: 10.1007/s00894-006-0149-4.
34 A. Michalak, M. Mitoraj and T. Ziegler, Bond Orbitals from Chemical Valence Theory, *J. Phys. Chem. A*, 2008, **112**, 1933–1939, DOI: 10.1021/jp075460u.
35 M. P. Mitoraj, A. Michalak and T. Ziegler, A Combined Charge and Energy Decomposition Scheme for Bond Analysis, *J. Chem. Theory Comput.*, 2009, **5**, 962–975, DOI: 10.1021/ct800503d.
36 T. Lu and F. Chen, Multiwfn: A multifunctional wavefunction analyzer, *J. Comput. Chem.*, 2012, **33**, 580–592, DOI: 10.1002/jcc.22885.
37 T. Lu, A comprehensive electron wavefunction analysis toolbox for chemists, Multiwfn, *J. Chem. Phys.*, 2024, **161**, 082503, DOI: 10.1063/5.0216272.
38 H. Zhao, J. Chang, A. Boika and A. J. Bard, Electrochemistry of High Concentration Copper Chloride Complexes, *Anal. Chem.*, 2013, **85**, 7696–7703, DOI: 10.1021/ac4016769.
39 K. Fagnou and M. Lautens, Halide Effects in Transition Metal Catalysis, *Angew. Chem., Int. Ed.*, 2002, **41**, 26–47, DOI: 10.1002/1521-3773(20020104)41:1<26::AID-ANIE26>3.0.CO;2-9.
40 A. N. Desnoyer, *et al.*, The Importance of Ligand-Induced Backdonation in the Stabilization of Square Planar d10 Nickel π-Complexes, *Chem.–Eur. J.*, 2019, **25**, 5259–5268, DOI: 10.1002/chem.201805987.
41 M. K. Khoshkbarchi and J. H. Vera, Measurement and correlation of ion activity in aqueous single electrolyte solutions, *AIChE J.*, 1996, **42**, 249–258, DOI: 10.1002/aic.690420121.
42 G. Wilczek-Vera, E. Rodil and J. H. Vera, On the activity of ions and the junction potential: Revised values for all data, *AIChE J.*, 2004, **50**, 445–462, DOI: 10.1002/aic.10039.
43 B. Saeednia, *et al.*, Unusually air-stable copper(i) complexes showing high selectivity for carbon monoxide, *Chem. Sci.*, 2025, **16**, 5058–5063, DOI: 10.1039/D5SC00237K.
44 E. I. Konnik, Salting-out and Salting-in of Gaseous Non-electrolytes in Aqueous Solutions of Electrolytes, *Russ. Chem. Rev.*, 1977, **46**, 577, DOI: 10.1070/RC1977v046n06ABEH002157.
45 L. Sun and J. Liang, Accurate prediction of carbon monoxide in aqueous solutions for geological sequestration applications, *Appl. Geochem.*, 2025, **187**, 106414, DOI: 10.1016/j.apgeochem.2025.106414.
46 M. Katsumoto, K. Kanehori and T. Kamiguchi, Carbon Monoxide Absorption by Aqueous CuCl-$MgCl_2$ Absorbent, *Bull. Chem. Soc. Jpn.*, 1984, **57**, 166–170.
47 W. D. Johnsen, *et al.*, Lewis Acids and Electron-Withdrawing Ligands Accelerate CO Coordination to Dinuclear CuI Compounds, *Inorg. Chem.*, 2023, **62**, 9146–9157, DOI: 10.1021/acs.inorgchem.3c01003.
48 D. Lionetti, S. Suseno, A. A. Shiau, G. de Ruiter and T. Agapie, Redox Processes Involving Oxygen: The Surprising Influence of Redox-Inactive Lewis Acids, *JACS Au*, 2024, **4**, 344–368, DOI: 10.1021/jacsau.3c00675.
49 M. Lundström, J. Aromaa and O. Forsén, Redox potential characteristics of cupric chloride solutions, *Hydrometallurgy*, 2009, **95**, 285–289, DOI: 10.1016/j.hydromet.2008.06.009.
50 G. Lacarbonara, N. Albanelli, D. Fazzi and C. Arbizzani, A spectroelectrochemical study of copper chloro-complexes for high performance all-copper redox flow batteries, *Electrochim. Acta*, 2023, **458**, 142514, DOI: 10.1016/j.electacta.2023.142514.
51 D. Tong, J. P. M. Trusler and D. Vega-Maza, Solubility of CO2 in Aqueous Solutions of CaCl2 or MgCl2 and in a Synthetic Formation Brine at Temperatures up to 423 K and Pressures up to 40 MPa, *J. Chem. Eng. Data*, 2013, **58**, 2116–2124, DOI: 10.1021/je400396s.
52 A. Schumpe, The estimation of gas solubilities in salt solutions, *Chem. Eng. Sci.*, 1993, **48**, 153–158, DOI: 10.1016/0009-2509(93)80291-W.

